CrossMark

Cu(II) adsorption from aqueous solutions using the inner and outer portions of sugarcane bagasse

Helen P. Toledo-Jaldin[1] · Alien Blanco-Flores[3,4] ·
Gustavo López-Téllez[2] 🔟 · Alfredo R. Vilchis-Nestor[2] ·
Víctor Sánchez-Mendieta[2] · Ernesto Morales-Almaraz[5] ·
Luis Alberto Mejía-Uribe[5]

Abstract

In the present work, the adsorption capacity of internal and external portions of treated sugarcane bagasse (SCB) to remove Cu(II) from aqueous solution was evaluated. In order to reuse this solid waste as an effective adsorption material, both portions were treated with three different solutions (hot water, ethanol and NaOH) to remove sugar, external gummy tissue and impurities. Adsorption experiments were carried out in a batch system at room temperature. The kinetic data were fitted to pseudo-second order and Elovich models for the internal portion, and to the Elovich model for the external portion reaching equilibrium times from 8 to 24 h. Freundlich and Langmuir–Freundlich models described well the adsorption behavior of all systems. The compositional differences of the two portions of SCB and the surface chemistry were analyzed. Material characterization by scanning electron microscopy, Fourier transformed infrared spectroscopy, and X-ray photoelectron spectroscopy demonstrated morphologic and chemical modifications of the material after each treatment. Results showed that external SCB treated with a sodium hydroxide solution and internal SCB treated with ethanol solution were the best adsorbent materials, and provided a surface with more affinity to remove Cu(II).

Keywords Kinetic and equilibrium isotherms · Cu(II) adsorption · Agro-waste · Morphological characterization

✉ Alien Blanco-Flores
blancoflores81@hotmail.com

✉ Gustavo López-Téllez
adramelyn@yahoo.com

Extended author information available on the last page of the article

🖄 Springer

Introduction

Pollution of aquatic environments is a major factor posing a serious threat to the survival of aquatic organisms, including those used as human food. Heavy metals are the most troublesome contaminants in waste water because unlike other species they are non-biodegradable. They may enter the aquatic environment from various sources, first from nature itself, but mainly from anthropogenic factors [1]. These contaminants are produced from a number of different activities such as manufacturing, metallurgy, mining, construction and incinerators [2].

As one of the great metals of commerce, it is not surprising that Cu(II) released by humans into the environment is in significant excess over what might be found naturally. Cu(II) pollution has occurred in the vicinity of mines and smelting operations since mankind began the activity several millennia ago [3]. Trace elements of Cu(II) are considered to be a potential biotoxin, mutagen and carcinogen; therefore, especially for water, Cu(II) and its compounds were ranked with the controlled contamination priority in several countries [4].

Cu(II) can poison microorganisms and accelerate the decomposition of aquatic organic matter; therefore water self-purification capability and ecology is greatly influenced. On the other hand, species used as food poisoned by Cu(II) threatens human health through bioaccumulation [5].

Furthermore, the huge amount of sugarcane bagasse (SCB) waste exhibits its own environmental problem. Its incorrect final disposition, very few developed commercial uses and little re-use applications make this large amount of waste a relevant environmental risk in countries such as México, where the annual production of sugar cane is around 22,951,682 tons per year [6]. In this context, some researchers have applied SCB in water pollution remediation as an effective adsorbent material for petroleum hydrocarbons removal [7], dye removal [8], and also activated carbon prepared from SCB was used for heavy metals adsorption [9]. In order to improve its adsorbent properties, several chemical methods were employed for the treatment, which includes phosphoric acid [10], formaldehyde and sulfuric acid [11], sodium hydroxide [12].

At this point, constant efforts are being made to solve and prevent hazards caused by Cu(II) in water sources. Some methods are available, including ion exchange [13], electrochemical systems [14], precipitation [15], co-precipitation [16] and adsorption. The latter has become a powerful tool for Cu(II) removal. The basic principle of adsorption is the transfer of the analyte from the aqueous phase to bind to active sites of the adjacent solid phase [17]. Adsorption is an attractive removal technique with some relevant advantages: the method is cheap, is user friendly, has good social acceptability, is easy to operate and maintain, there is no daily sludge disposal problem, it has lower consumption of reagents and is particularly environment friendly [18]. Various synthesized composites have been successfully used for Cu(II) removal such as chitosan-clay nanocomposites [19], chitosan/MWCNT/Fe3O4 composite [20], carboxymethyl cellulose/sodium styrene sulfonate gels [21], but biosorption is an attractive alternative due to its effectiveness in reducing the concentration of heavy metal ions to very low levels and the use of

inexpensive biosorbent materials. The presence of compounds such as cellulose, hemicellulose and lignin, with binding sites capable to take up metals, suggests the valorization of SCB by-products as a low cost natural and green biosorbent [22]. Moreover, the present work considers the separation of this residue into its external and internal portions to prove that htey are absorbent materials, separately. This separation has not been reported so far in any previous work.

In this context, the adsorption of Cu(II) was evaluated using SCB after three different treatments with hot water, ethanol and sodium hydroxide solutions. The SCB was separated and analyzed as two different portions [internal (IB_N) and external (EB_N)]. The adsorption process was investigated in batch mode and mathematical models were applied in order to analyze the removal dynamics.

Materials and methods

Reagents

All the chemicals used in present study were of analytical reagent grade. NaOH was supplied by Merck Chemie assay $\geq 99.0\%$ and ethanol (assay $\geq 50\%$) by REASOL. Ammonia hydroxide (NH_4OH assay 63%) was purchased from Fermont. Copper stock solution of 1000 mg/L was prepared from copper nitrate [$Cu(NO_3)_2 \cdot 2.5H_2O$ Fermont, assay 99.4%], and necessary dilutions were done with deionized water.

Adsorbent preparation

SCB was obtained from a local juice center in Veracruz, México. The material was sun-dried for 5 days. Internal natural SCB (IB_N) and external natural SCB were set apart manually (EB_N), grounded and sieved in order to obtain a more homogeneous particle size ranging between 0.707 and 0.841 mm.

IB_N and EB_N were subject to three different treatments in order to eliminate contaminants, sugars and gummy tissue. A fraction of IB_N and EB_N was washed with hot water under 80 °C, another one with sodium hydroxide (NaOH) solution at 0.05 M and the last one with ethanol at 10% v/v for 24 h. After this time samples were filtered, well dried and powdered before use. After the treatments the inner and outer portions of SCB were labeled as IB_W, IB_{OH}, IB_{Eth} and EB_W, EB_{OH}, EB_{Eth} from the treatment with hot water (W), sodium hydroxide (OH) and ethanol solution (Eth), respectively.

Characterization

Acid detergent fiber (ADF), neutral detergent fiber (NDF) and acid detergent lignin (ADL) of the inner and outer portions of the SCB were determined according to Van Soest et al. [23]. ADF corresponds to cellulose and lignin, NDF contains cellulose and lignin, as well as hemicellulose, and ADL is the lignin portion.

Point of zero charge and concentrations of the acid–base groups were determined according to Blanco-Flores et al. [24]. The zero charge point was established mixing each material with 0.01 M NaCl solutions adjusting the pH values between 2 and 12 by adding 0.1 M HCl or NaOH solutions. After 24 h of contact, samples were centrifuged, decanted, and pH was analyzed in the final liquid phases with a Conductronic pH 120 instrument.

Determination of superficial chemistry was done as follows: for the superficial basicity, samples of 0.2 g of each material were put in contact with 25 mL of 0.025 M HCl solution and shaken for 24 h and at 120 rpm. After that time, the samples were decanted and the excess acid was titrated with 0.025 M NaOH. The superficial acidity was obtained by a similar procedure, where a 0.025 M NaOH solution was put in contact with each material and the solution titration was performed using 0.025 M HCl. The experiments were done in duplicate.

Infrared absorption spectra (FTIR) were applied on the SCB before and after the treatment. A Bruker (model Tensor-27) ATR FT-IR infrared spectrometer was used to elucidate the functional groups present in each material. The software ORIGIN 8.0 was used to create all figures. The surface morphology was investigated after and before every treatment using a scanning electron microscope (Philips, XL-30) operated at 20 kV. Samples were fixed on a support with a carbon film and sputter-coated with gold. The X-ray photoelectron spectroscopy (XPS) wide and narrow spectra was acquired using a JEOL JPS-9200, equipped with a Mg X-ray source (1253.6 eV) at 200 W, the area of analysis was 3 mm^2, pass energy of 15 eV, and the vacuum was in the order of 7.5×10^{-9} Torr for all samples. The spectra was analyzed using the Specsurf^{TM} software included with the instrument; all spectra were charge-corrected by means of the adventitious carbon signal (C1s) at 284.5 eV. The Shirley method was used for the background subtraction, whereas for the curve fitting the Gauss-Lorentz method was used.

The suspensions were filtrated and supernatants concentrations were determined by a spectrophotometer (UV–Vis Perkin Elmer Lambda 10) at 600 nm.

Adsorption kinetic experiments

Adsorption experiments were conducted under static conditions by the batch equilibrium technique by adding 2.0 g of treatment material (IB_W, IB_{OH}, IB_{Eth}, EB_W, EB_{OH} and EB_{Eth}) to 200 mL of Cu(II) solution 800 mg/L with constant stirring at room temperature. This concentration was used based on a previous work by Dos Santos et al. [12]. At certain moments (0.25, 0.5, 1, 2, 4, 6, 8, 16, 18, 20, 22, 24, 40 and 48 h), aliquots of the solution were taken and filtered, and each experimental point was measured twice. Although the pH of the solution is an important variable in the adsorption of Cu(II), the pH of the solution was not adjusted because for all tests it did not vary significantly from the initial value (pH = 4.0 ± 0.2). The supernatant was tested with a UV–Vis spectrophotometer [25] for metal residual quantification at 600 nm. In order to verify if there was anything that could interfere in the supernatant quantification, a blank run was conducted. In this test, the same quantity of material was used in contact with 200 mL of distilled water.

The amount of adsorbed metal per gram of material (q_t) as a function of time (t) was calculated as the following:

$$q_t = \frac{(C_0 - C_t) \times V}{m} \qquad (1)$$

where C_0 is the initial metal concentration and C_t is the concentration after contact time (mg/L), V is the solution volume (L), and m the SCB mass (g). Models tested were pseudo-first order, pseudo-second order, second order and intra-particle diffusion models [24].

Adsorption isotherms

Adsorption isotherms of Cu(II) on IB_W, IB_{OH}, IB_{Eth}, EB_W, EB_{OH} and EB_{Eth} were determined under the same batch conditions. Solutions of Cu(II) ions at different concentrations were prepared, ranging from 100 to 800 mg/L. Afterwards, 5 mL of each concentration of Cu(II) solutions were individually used and agitated with 50 mg of SCB, each material at the equilibrium time determinate previously. Next, the mixtures were separated by filtration and the solutions were analyzed by UV–Vis spectrophotometer.

Equation 1 was used, the amount of adsorbed metal per gram of SCB was calculated and a plot of qe in function of Ce was built. The models tested were Langmuir, Freundlich, Langmuir–Freundlich and Temkin [25] since they are the models most often mentioned in the literature to describe adsorption processes in liquid phase. Langmuir model was used to establish the maximum adsorption capacity of the adsorbent (q_m) since this model assumes that a monolayer is formed over the surface of the adsorbent material when it gets saturated [26].

Results and discussion

Adsorbent characterization

The SCB is mainly composed of cellulose (Ce), hemicellulose (He) and lignin (L). Its composition varies according to the place of origin and the conditions of culturing. Therefore, many attempts have been made to characterize this natural material but since it is mainly used as a whole the inner and outer portions are not consider separately. In Table 1 the acid detergent fiber (ADF), neutral detergent

Table 1 Chemical composition of sugarcane bagasse, inner and outer portions

Material	% NDF (Ce + He + L)	% ADF (Ce + L)	% ADL (L)
SCB	59.45 ± 0.373	34.91 ± 0.183	5.65 ± 0.130
IB_N	54.88 ± 0.204	28.94 ± 0.001	2.24 ± 0.001
EB_N	62.52 ± 0.297	39.91 ± 0.377	6.54 ± 0.143

fiber (NDF) and acid detergent lignin (ADL) of the SCB, IB_N and EB_N portions were determined. The first one was compared with SCB from Brazil characterized by Guimarães et al. [27]. All the fractions were higher, which was expected since they are from different crops conditions. However knowing the composition of each portion was very important since lignin has a highly resistant structure and the treatments may be less aggressive to the portions with the highest content of lignin. The results showed a larger amount of lignin in the outer portion than in the inner.

Point of zero charge (pH_{PZC}) and the final pH for each material after the contact is in Table 2. At this pH value the charge of each material will be zero and above this pH bagasse will have a negative charge [1]. Therefore, it is clear that in all materials the adsorption of cations such as Cu(II) is favoured since the $pH_{final} > pH_{PZC}$. The values of the inner portions are higher than the values of the external. The surfaces of the external portions are more negatively charged than the internal portions. These superficial characteristics can be modified after the treatments since the values of IB_N and EB_N are higher even after the treatment with hot water. Zhang et al. [28] determined a pH_{PZC} of 5.0 for natural bagasse washed with distilled water to remove sugars and ash components and air-dried to constant weight. This value is close to the internal and external material hot water washed (IB_W and EB_W). The concentrations of the acid and base groups (Ca and Cb, respectively) are detailed in Table 2. The concentration of acid groups is less than the concentration of base groups in both portions of the natural SCB (IB_N, EB_N). After the inner portion treatments, acid and base concentrations increased. In case of the outer portion the concentration of base groups increased, while the acid groups decreased or remained constant. This points out the different responses of the inner and outer portions surfaces of the SCB to the tested treatments. Since the base groups are more than the acid groups, the surface characteristic is in general basic, it was reinforced by the pH_{PZC} values less than 7. A negative structural charge at the surface of the material strongly adsorbs cations [29] like Cu(II).

Figure 1 shows the infrared spectra of IB_N, IB_W, IB_{OH}, IB_{Eth}, EB_N, EB_W, EB_{OH} and EB_{Eth}. The strong signal at 3312–3347 cm^{-1} is typical from cellulose [7] hemicellulose and lignin correspond to the presence of stretching vibration –OH. Bands at 2837–2913 cm^{-1} are characteristics of stretching vibration C–H of methylene and methyl groups of lignin. The signal between 1603 and 1608 cm^{-1} is due to carboxylic groups present in lignin and hemicellulose. Four weak bands around 1450, 1500, 1580 and 1600 cm^{-1} represent the C=C vibration in the

Table 2 Point of zero charge and acid–base groups concentrations of each material

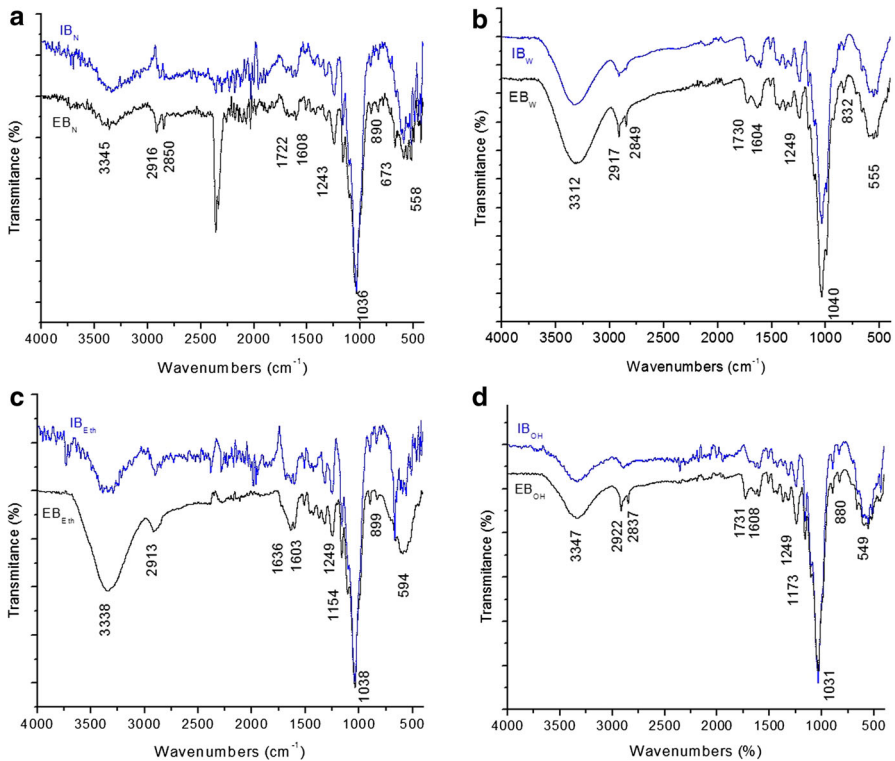| Material	IB_N	IB_W	IB_{OH}	IB_{Eth}	EB_N	EB_W	EB_{OH}	EB_{Eth}
pH_{final}	7.16	7.18	7.19	7.24	6.67	6.93	7.15	7.04
pH_{PZC}	4.58	5.13	5.98	5.94	6.02	5.67	6.03	6.06
Cb (meq/g)	0.045	0.050	0.060	0.050	0.050	0.060	0.055	0.055
Ca (meq/g)	0.013	0.024	0.018	0.023	0.024	0.018	0.016	0.024

Fig. 1 Infrared spectra of IB_N–EB_N (**a**); IB_W–EB_W (**b**); IB_{Eth}–EB_{Eth} (**c**) and IB_{OH}–EB_{OH} (**d**)

aromatic rings of lignin. The strong signal at 2320 cm^{-1}, which correspond to EB_N, is related to CO_2.

The strong signal at 1040–1031 cm^{-1} represents the C–O vibration. The adsorption band at 890 cm^{-1} represents the β-glycoside linkages (1 → 4) [30]. The band at 1722–1731 cm^{-1} is characteristic of C=O carbonyl group.

The treatment of SCB with NaOH solution is used to extract no cellulosic binding materials such as hemicellulose and lignin complexes as established by Abdel-Halim [31]. In the same way, the treatment with ethanol reduces the lignin concentration increasing the cellulose percentage according to Salcedo Mendoza et al. [32]. The signal of –OH is less intense after the treatment of IB_{OH}, EB_{OH} and IB_{Eth} compared to IB_W and EB_W. This could be a consequence of the extraction of hemicellulose and lignin since both have –OH groups, which might contribute to the intensity of the signal. The low concentration of NaOH and ethanol solutions may be enough to reach this phenomenon. On the other hand, the same signal for EB_{Eth} increases and the signal around 1730 cm^{-1}, related to lignin, is not visible, this can be explained by the enzymatic hydrolysis. Mesa et al. [33] treated SCB with ethanol in a reactor at high temperature pursuing this phenomenon. In our case, the enzymatic hydrolysis is less intensive because the conditions are different and less

aggressive for the material; however, the phenomenon takes place and is verified by the EB_{Eth} spectroscopy behavior.
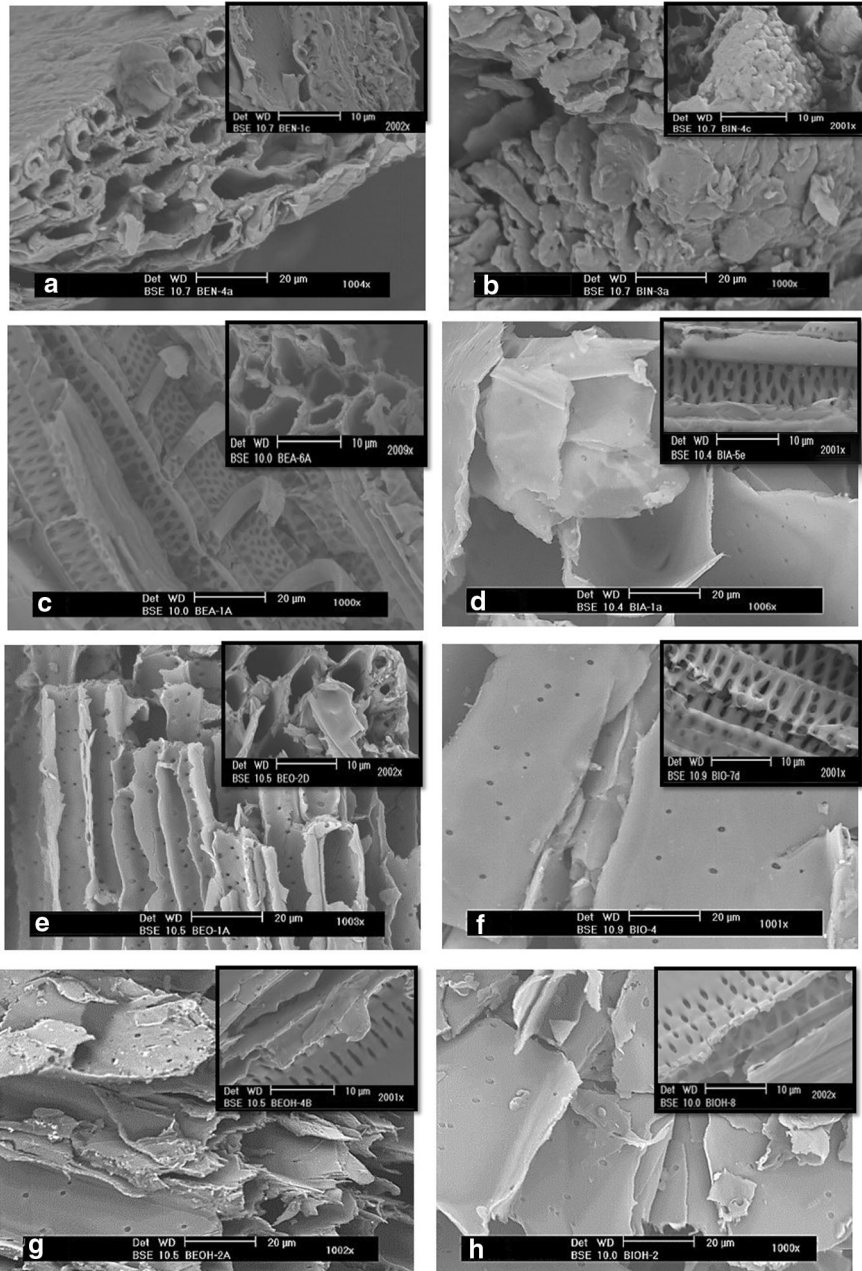

Fig. 2 SEM images of EB_N (**a**); IB_N (**b**); EB_W (**c**); IB_W (**d**); EB_{Eth} (**e**); IB_{Eth} (**f**); EB_{OH} (**g**); IB_{OH} (**h**)

Internal and external SCB after treatment were analyzed by scanning electron microscopy (SEM); images are shown in Fig. 2. These figures reveal the surface texture and porosity at $1000\times$ and $2000\times$ magnification. Some debris clearly showed up when we analyzed SEM images of EB_N and IB_N (Fig. 2a, b). In the case of IB_N they appear on layers surface and blocking channels of EB_N. This information is relevant because it supports the fact that SCB needs to be treated before it can be used as absorbent material. In SEM images of EB_W, EB_{Eth} (Fig. 2c, e) some channels are easily identifiable; however, they are compromised when the material is treated with NaOH (Fig. 2g). In this last material, the channel structure looked collapsed and some of them may even disappear. Nevertheless, pores with large dimensions are identified, which is probably why, despite the morphology modification, the material maintains its adsorbent properties. In the case of internal SCB IB_W, IB_{OH} and IB_{Eth} (Fig. 2d, f, h) the structure seems to be made of overlapped layers unlike external SCB. Micrographs at $2000\times$ magnification (Fig. 2d, f, h) exposed a hive structure formed by consecutive pores under layers, which can be seen on the layers surface such as disperse pores. The internal SCB structure of the material treated with NaOH (IB_{OH}) seems to be more compromised than the external one. This could be because the external portion has more lining and its structure is more resistant than cellulose and hemicellulose. It means that the layer structure seems to be broken, pointing out a modification that did not occur after the others treatments. As Loh et al. [34] established, treatment with hot water and ethanol could reduce gummy tissue and debris attached on the fiber with no morphology modification.

Treatment with NaOH solution is aggressive for internal and external SCB compromising the structure of the material. Pores in different shapes and sizes could be observed in external, as well as in internal SCB and may contribute to Cu(II) adsorption.

XPS was used to determine the oxidation state of copper after removal process. A large and distinct peak can be seen in the Cu $2p_{3/2}$ core region at energy level near to 932 eV. The copper and oxygen curve fitting spectra are presented in Fig. 3. The corresponding binding energies with relative content of copper species are listed in Table 3.

The curve fitting spectra of EB_{OH} (Fig. 3a) shows five peaks: 930.66 and 931.46 eV can be attributed to Cu(I) interacting with oxygen, one probably forming Cu_2O. It is important to mention that the binding energy reported for this compound is 932 eV; however, a lower energy might mean a weak interaction of Cu(I) with oxygen, since it is necessary a lower energy to move electrons from it. This was verified by oxygen spectra in Fig. 3b. Two signals (528.95 and 529.41 eV) are related to Cu_2O at lower energies than the reported. The chemical state of Cu(II) was confirmed by peaks at 932.58, 933.86 and 934.89 eV, the first one corresponds to $Cu(OH)_2$ and the others to CuO. Their presence was verified by four peaks between 529.91 and 531.79 eV in oxygen spectra. According to Pereira et al. [35] and Zhong et al. [36] peaks between 532.41 and 533.95 eV can be assigned to O=C, –C–OH, –C–O– and O–C=O of cellulose, hemicellulose and lignin of the SCB.

The curve fitting spectra for IB_{Eth} (Fig. 3c) registered five peaks, one of which is related to Cu(I) at 932.40 eV; the other four peaks suggested the presence of Cu(II).
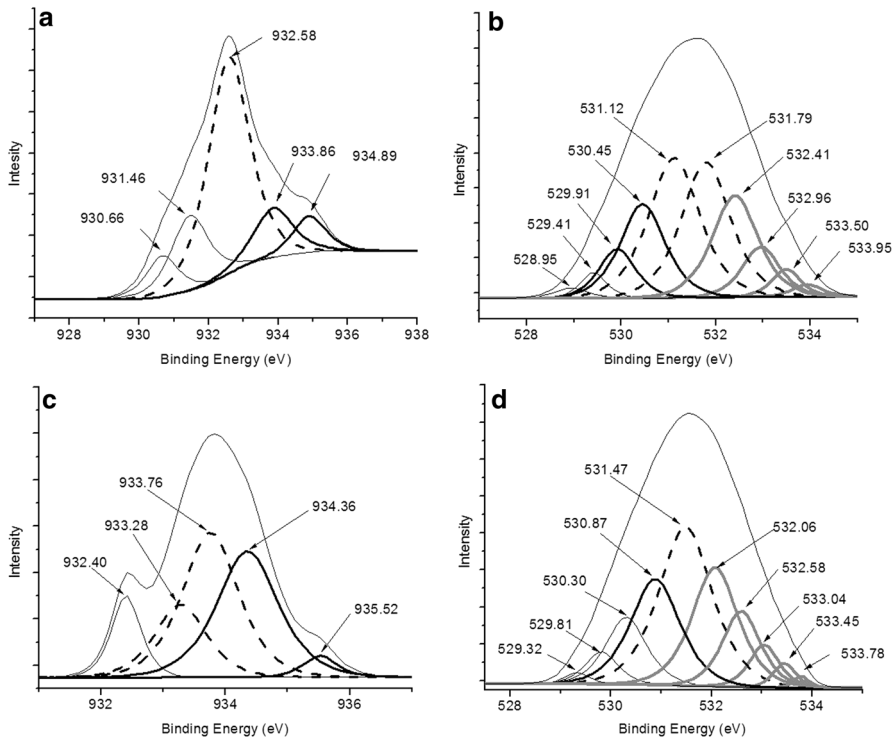
Fig. 3 XPS curve fitting scan of Cu $2p_{3/2}$ and O 1s in EB_{OH} (**a, b**) and IB_{Eth} (**c, d**)

Table 3 Binding energy for copper different states of oxidation and relative content

Chemical state	Formula	Binding energy (eV)	Content (%)
BE_{OH}			
Cu(I)	Cu_2O	930.66	7.96
Cu(I)	Cu_2O	931.46	17.46
Cu(II)	CuO	932.58	55.50
Cu(II)	$Cu(OH)_2$	933.86	11.94
Cu(II)	$Cu(OH)_2$	934.89	7.15
IB_{Eth}			
Cu(I)	Cu_2O	932.40	10.48
Cu(II)	CuO	933.28	16.58
Cu(II)	CuO	933.76	35.86
Cu(II)	$Cu(OH)_2$	934.36	33.97
Cu(II)	$Cu(OH)_2$	935.52	3.11

Peaks at 933.28 and 933.76 eV correspond to CuO and can be correlated to the O 1 s signal at 531.47 eV; the largest peak in the curve fitting spectra for O 1s in Fig. 3d. The peak at 932.40 eV is attributed to Cu(I) interacting with oxygen and is related to three low peaks at 528.95, 529.41 and 530.30 eV in oxygen curve fitting.

Adsorption kinetics

Equilibrium time was determined from the plot of t versus q_t. The graphical behaviour of all materials was similar; however, regarding equilibrium times they were achieved at different times as can be seen in Table 4.

In order to describe the adsorption dynamics mathematically four kinetic models were applied: pseudo-first order, pseudo-second order, Elovich and intra-particle diffusion. The Figs. 4, 5 and 6 show the kinetic experimental data and the applied mathematical models for each adsorbent material. Tables 5 and 6 shows the parameters and values of three kinetic models.

In the case of IB_W, IB_{OH}, IB_{Eth} the treatment was remarkable, since different models described the process for each material, unlike for external material. For IB_W the process was described by pseudo-second order model, which means that the process of Cu(II) adsorption is chemical adsorption, which includes valence forces with the exchange of ions or the formation of covalent bonds [37]. This statement can be related to XPS results, where valence forces were found. For IB_{Eth} the best-fitted equation is a pseudo-first order model; however, according to Gupta et al. [38] this equation does not fit well in the whole range of interaction time. For this reason and for the closest value of R^2, the best-fitted equation was established as a pseudo-second order model. In the case of IB_{OH} Elovich model fitted well with experimental data. The Elovich equation assumes that the actual solid surface is energetically heterogeneous and that neither desorption nor interactions between the adsorbed species could substantially affect the kinetics of adsorption at low surface coverage [38]. It is important to mention that the Elovich model describes a very heterogeneous surface that may result from the aggressive treatment, as can be supported by the SEM characterization. Both IB_W and IB_{OH} adsorbed Cu(II) faster since values of K_2, from the pseudo-second order model, are in accordance with the equilibrium time found previously (8 h). The material with the lowest value of K_2 is IB_{Eth} and simultaneously has the highest value of equilibrium time (24 h). This results were consistent with previous observations of adsorption Cu(II) on SCB treated with NaOH [12]. All other results were not compared due to a lack of previous research using hot water and ethanol for treatment of SCB.

The best correlation is observed between external SCB experimental data (EB_W, EB_{Eth} and EB_{OH}) and the Elovich model with R^2 higher than 0.969. None of the adsorption kinetics data of these materials fit the pseudo-first order model, although R^2 values are close to the pseudo-second order model. This suggests that a chemical process might control the adsorption. This is consistent with Tejada et al. [39], who established that ionic metals removal from water solutions by bio-adsorption generally depends on the chemical mechanisms that involve interaction of ionic metals with active groups in the bio-adsorbent. XPS results verify strong covalent interactions between copper and oxygen. According to Elovich model the

Table 4 Equilibrium time for each material

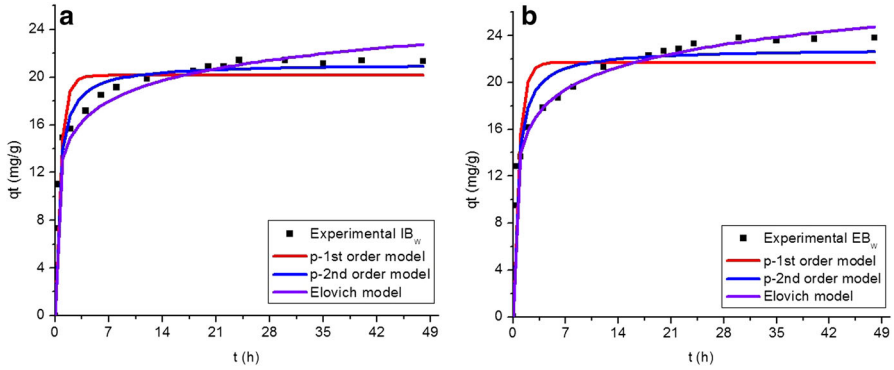| Material	IB_W	IB_{OH}	IB_{Eth}	EB_W	EB_{OH}	EB_{Eth}
Equilibrium time (h)	8	8	24	16	16	16

Fig. 4 Adsorption kinetics of Cu(II) on **a** IB$_W$ and **b** EB$_W$
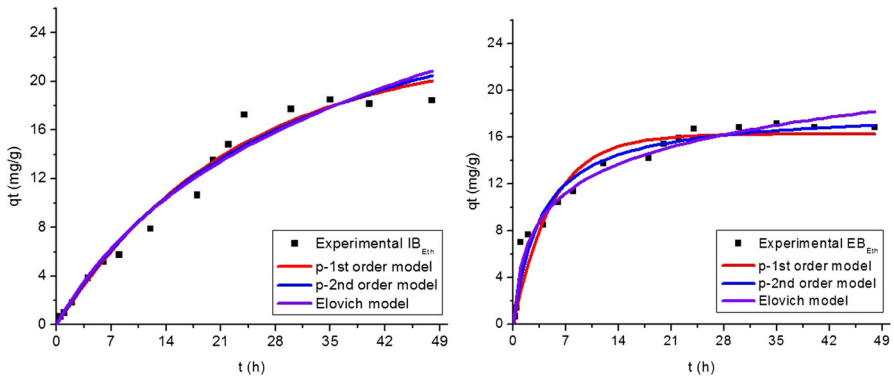

Fig. 5 Adsorption kinetics of Cu(II) on **a** IB$_{Eth}$ and **b** EB$_{Eth}$
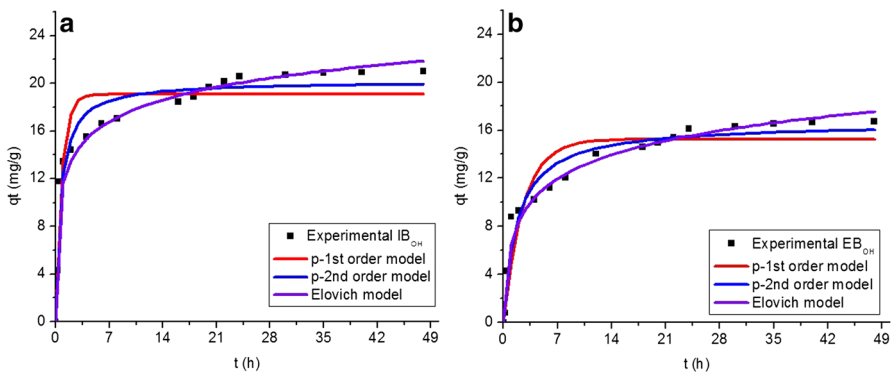

Fig. 6 Adsorption kinetics of Cu(II) on **a** IB$_{OH}$ and **b** EB$_{OH}$

Table 5 Parameters in the kinetic equations for Cu(II) adsorption with treated internal SCB

Models	Parameters	IB_W	IB_{Eth}	IB_{OH}
Pseudo-first order	q_t (mg/g)	20.14	22.71	19.02
	K_1 (min^{-1})	1.38	0.045	1.24
	R^2	0.937	0.975	0.894
	RSS	34.003	20.554	57.943
	X^2	2.266	1.370	3.863
Pseudo-second order	q_t (mg/g)	21.11	33.71	20.17
	K_2 (g/mg h)	0.093	0.001	0.079
	R^2	0.984	0.971	0.949
	RSS	8.437	24.22	27.93
	X^2	0.562	1.614	1.862
Elovich	α (mg/g)	510.6	1.186	216.34
	β (mg/g)	0.404	0.084	0.379
	R^2	0.971	0.966	0.957
	K_2	15.88	27.76	23.65
	RSS	1.059	1.851	1.577

Table 6 Parameters in the kinetic equations for Cu(II) adsorption with treated external SCB

Models	Parameters	EB_W	EB_{Eth}	EB_{OH}
Pseudo-first order	q_t (mg/g)	21.71	16.23	15.25
	K_1 (min^{-1})	1.305	0.197	0.394
	R^2	0.862	0.942	0.9003
	RSS	87.46	31.91	44.79
	X^2	5.83	2.13	2.99
Pseudo-second order	q_t (mg/g)	22.86	18.26	16.60
	K_2 (g/mg h)	0.08	0.015	0.034
	R^2	0.946	0.968	0.956
	RSS	34.61	17.811	19.77
	X^2	2.31	1.19	1.32
Elovich	α (mg/g)	428.02	10.45	24.77
	β (mg/g)	0.36	0.271	0.34
	R^2	0.995	0.973	0.969
	RSS	3.38	15.08	14.11
	X^2	0.23	1.01	0.94

controlling mechanism for the adsorption corresponds to a second-order reaction with a heterogeneous adsorbent surface and different activation energies. Only one model describes adsorption process for all external materials probably because treatments were not aggressive enough to modify the materials. According to this model α and β represent the initial adsorption rate (mg/g h) and the desorption constant (g/mg), respectively [40]. In all cases, β values are low, meaning that the adsorption process is more intense than desorption. On the other side, α for EB_{Eth}

and IB$_{Eth}$ have the lowest initial adsorption rate, which is congruent with a lower slope during the initial times of the adsorption process.

Intra-particle diffusion parameters were calculated in order to determine the rate limiting step. Figures 7, 8 and 9 show the found regions for each adsorbent material. Three distinct adsorption regions were identified in each intra-particle diffusion plots and the parameters are in Table 7. The first linear segment is attributed to the boundary layer diffusion caused by the transfer of molecules from the liquid solution to the outer surface of the adsorbent and the second region corresponds to the intra-particle pore diffusion in which molecules diffuse throughout the porous surface of the material [41].

Since none of the plots pass through the origin, it may be concluded that intra-particle diffusion is not the only rate-controlling step for the sorption of copper, film diffusion could be also operating simultaneously during the process [42].

The application of this model showed that treatment of the internal SCB was significant, liquid film diffusion was influential in the copper adsorption process, the treatment with ethanol resulted in a ticker liquid film ($C = 30.14$ mg/g). For the rest of materials, the model suggested that the intra-particle diffusion is the rate-limiting step.

Adsorption isotherms modeling

Conventional batch method was performed in order to evaluate the maximum adsorption capacity of each material for Cu(II) ions removal.

For initial concentrations of 100 mg/L average removal efficiency above $90 \pm 5\%$ was achieved for IB$_W$, IB$_{OH}$, IB$_{Eth}$, EB$_{OH}$ and EB$_{Eth}$. When the initial concentration of Cu(II) in solution was higher than 100 mg/L the removal percentages were lower, meaning that the removal efficiency was enhanced at lower initial concentrations. This could be the result of a solid interface negative charged and the formation of a Stern layer positive charged. A double layer may be formed in order to neutralize the charged surface causes an electrokinetic potential between the surface and any point in the mass of the suspending liquid [43]. Nevertheless, if
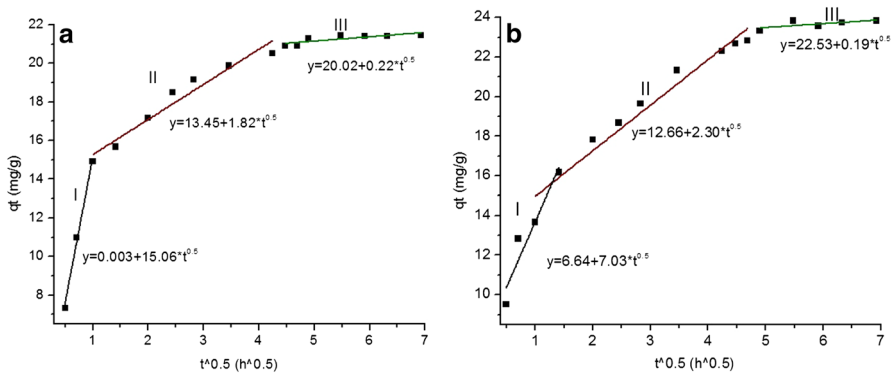

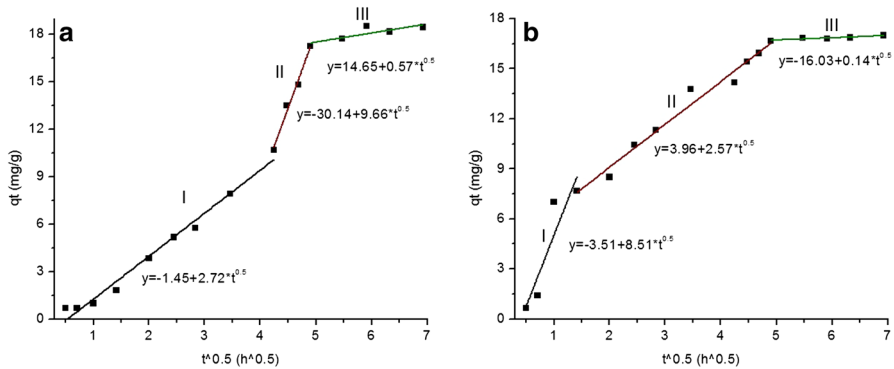**Fig. 7** Intra-particle diffusion model of **a** IB$_W$ and **b** EB$_W$

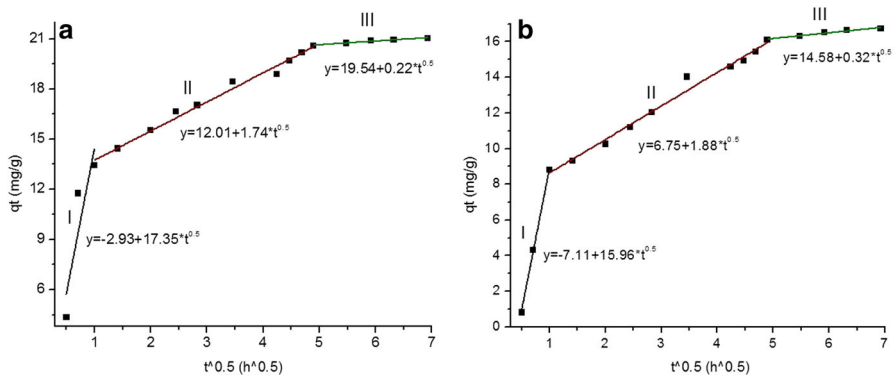Fig. 8 Intra-particle diffusion model of **a** IB_{Eth} and **b** EB_{Eth}

Fig. 9 Intra-particle diffusion model of **a** IB_{OH} and **b** EB_{OH}

the positive charged of the Stern layer exceed the negative charged of the solid interface a repulsion interactions at long range tends to be dominated by an electrostatic double-layer repulsion [44].

The obtained values from each model applied to isotherm data are listed in Table 8. Figures 10, 11 and 12 show the experimental results and mathematical models for each adsorbent material. Preliminarily, according to the Langmuir model, the highest adsorption capacity was achieved for $IB_{Eth\ and}\ EB_{OH}$. This means that the chemical treatment with NaOH solution improved the adsorbing properties of the external part of the SCB while the treatment with ethanol is efficient for the internal portion of the SCB. The close to unity values of the regression coefficient (R^2), the sum of squared deviations of the points from the regression curve (RSS) and squared chi (X^2) indicated good fitting of the Langmuir–Freundlich model for EB_W and Freundlich for the other materials describing an adsorption process through diverse mechanisms and on heterogeneous surfaces, respectively. For each material the value $1/n$ was between 1 and 0, which means that the process is favorable [45]. On the other hand, the close to zero value of $1/n$ showed that the more heterogeneous materials are EB_W and IB_{Eth}. This is consistent since the

Table 7 Intra-particle diffusion model parameters for inner and outer portions of the sugarcane bagasse

Models	Stage	Parameters	EB_W	EB_{Eth}	EB_{OH}
Intraparticle diffusion	I	K_d (mg/g*min$^{0.5}$)	7.03	8.51	15.95
		C (mg/g)	6.64	-3.51	-7.11
		R^2	0.868	0.777	0.999
	II	K_d (mg/g*min$^{0.5}$)	2.30	2.57	1.88
		C (mg/g)	12.66	3.96	6.75
		R^2	0.952	0.978	0.986
	Stage	Parameters	IB_W	IB_{Eth}	IB_{OH}
	I	K_d (mg/g*min$^{0.5}$)	15.06	2.72	17.35
		C (mg/g)	0.003	1.45	2.93
		R^2	0.987	0.981	0.623
	II	K_d (mg/g*min$^{0.5}$)	1.82	9.66	1.74
		C (mg/g)	13.47	-30.14	12.01
		R^2	0.940	0.977	0.986

external SCB treated with water did not showed a significant modification (as might be inferred from characterization), and the internal SCB treated with ethanol may have a heterogeneous morphology, which can contribute to the adsorption process (since this has a major adsorption capacity).

Since the Langmuir isotherm model is based on the assumptions that a homogeneous monolayer on the material correspond to the maximum adsorption capacity [46], the adsorption capacity corresponds to $IB_{Eth} > IB_{OH} > IB_W$ and $EB_{OH} > EB_{Eth} > EB_W$. For the Freundlich model K_F is the magnitude related to the adsorption capacity of Cu(II) ions and is in agreement with Langmuir isotherm observations. The empirical parameter K_L is related to the intensity of adsorption and according to this parameter, there are stronger interaction forces between adsorbate and adsorbent between copper and internal SCB materials.

The obtained values of adsorption capacity around 22.93 mg/g for EB_{OH} and 23.93 mg/g for IB_{Eth} show that treated SCB has a great potential to remove Cu(II) from aqueous solutions. A comparison is described in Table 9. The results also show that the treatment, even with hot water, improves the adsorption capacity of the SCB since Dos Santos et al. [12] found lower adsorption capacity for natural SCB 6.87 mg/g. However, they established 31.53 mg/g as the adsorption capacity of SCB treated with citric acid. Yu et al. [47] applied unmodified and modified sugarcane bagasse for copper removal. The modification was made by pyromellitic dianhydride. The adsorption capacity of the modified SCB was 76.88 mg/g; however, the maximum capacity of the unmodified SCB was only 6.36 mg/g, less than for EB_{OH} and for IB_{Eth}. The modification increases the capacity of the material, but it requires the use of an organic compound. Iqbal et al. [48] removed 13.007 mg/g of Cu(II) using *Fumaria indica* biomass without modification, only half of the

Table 8 Isotherm modeling parameters

Models	Parameters	EB_W	EB_{Eth}	EB_{OH}
Langmuir	q_m (mg/g)	8.33	19.95	22.93
	b (L/mg)	0.011	0.004	0.005
	R^2	0.920	0.920	0.765
	RSS	1.58	10.88	39.88
	X^2	0.198	1.36	4.98
Freundlich	$1/n$	0.29	0.44	0.40
	K_F (mg/g)(L/mg)$^{1/n}$	0.89	1.15	1.36
	R^2	0.955	0.957	0.913
	RSS	0.877	5.85	14.78
	X^2	0.110	0.731	1.847
Langmuir–Freundlich	q_m	13.47	84.89	189.9
	K (mg/g)	0.046	0.009	0.007
	$1/n$	0.51	0.495	0.417
	R^2	0.960	0.948	0.894
	RSS	0.691	6.186	15.68
	X^2	0.099	0.884	2.24
Temkin	a (mg/g)	0.18	0.24	0.302
	b (mg/g)	1.55	2.59	2.97
	R^2	0.952	0.780	0.747
	RSS	0.937	29.98	42.91
	X^2	0.117	3.75	5.36

Models	Parameters	IB_W	IB_{Eth}	IB_{OH}
Langmuir	q_m (mg/g)	16.57	23.29	20.40
	b (L/mg)	0.087	0.025	0.017
	R^2	0.779	0.796	0.724
	RSS	22.02	52.28	45.02
	X^2	2.75	6.54	5.63
Freundlich	$1/n$	0.312	0.261	0.281
	K_F (mg/g)(L/mg)$^{1/n}$	1.99	4.43	3.286
	R^2	0.888	0.976	0.921
	RSS	11.18	6.26	12.94
	X^2	1.40	0.781	1.62
Langmuir–Freundlich	q_m	71.53	109.4	101.5
	K (mg/g)	0.025	0.039	0.030
	$1/n$	2.82	3.24	3.08
	R^2	0.788	0.968	0.904
	RSS	11.51	7.20	13.61
	X^2	1.64	1.03	1.94

Table 8 continued

Models	Parameters	IB_W	IB_{Eth}	IB_{OH}
Temkin	a (mg/g)	0.551	0.928	0.458
	b (mg/g)	2.27	3.56	3.36
	R^2	0.782	0.914	0.855
	RSS	21.68	22.02	23.65
	X^2	2.71	2.75	2.96
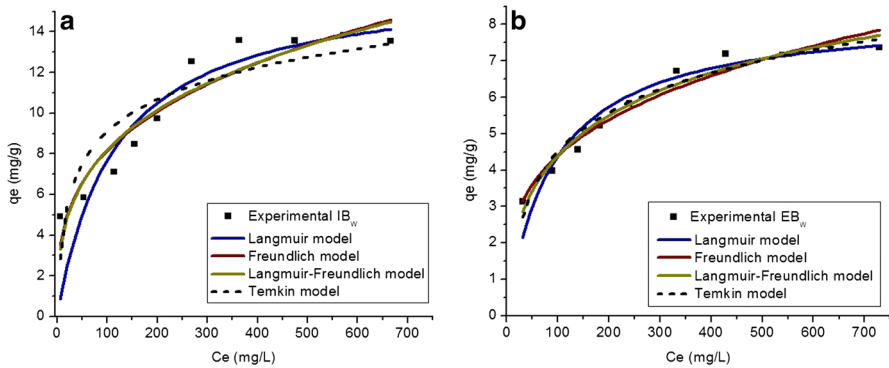
Fig. 10 Adsorption isotherms of metal copper on **a** IB_W and **b** EB_W
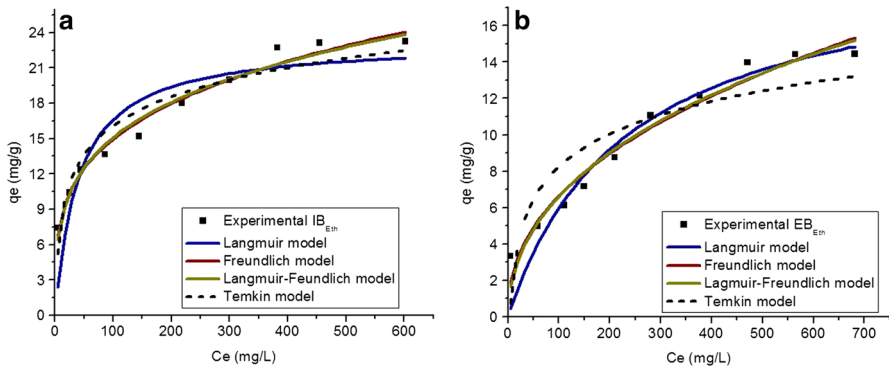
Fig. 11 Adsorption isotherms of metal copper on **a** IB_{Eth} and **b** EB_{Eth}

capacity of our materials. A closer result was found by Gupta and Ultrason [49], who removed 27.07 mg/g of Cu(II) using watermelon treated with citric acid. However, Ben-Ali et al. [50] washed, dried and sieved pomegranate peel as adsorbent material for Cu(II) removal. The found adsorption capacity was 30.12 mg/g, but they needed to adjust the pH and increase the temperature to 40 °C. It is important to mention that the research where SCB was applied as adsorbent material, with or without modification, did not separate the bagasse.
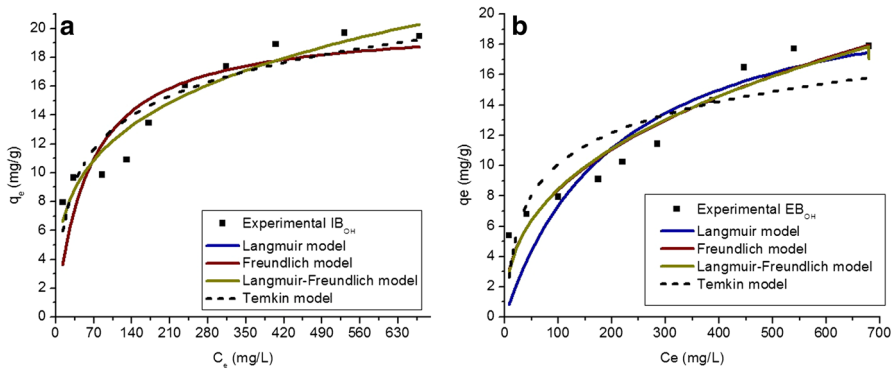
Fig. 12 Adsorption isotherms of metal copper on **a** IB_{OH} and **b** EB_{OH}

Table 9 Comparison of the maximum adsorption capacity with other biomass

Author	Material	q_{max} (mg/g)
Present research	EB_W	8.33
	EB_{Eth}	19.95
	EB_{OH}	22.93
	IB_W	16.57
	IB_{Eth}	23.93
	IB_{OH}	20.40
[12]	Natural sugarcane bagasse	6.87
	Modified bagasse with nitric acid	31.53
[47]	Pyromellitic dianhydride modified sugarcane bagasse	76.88
	Natural sugarcane bagasse	6.36
[48]	*Fumaria indica* biomass	13.007
[49]	Watermelon treated with citric acid	27.027
[50]	Pomegranate peel	30.12

Therefore, the characteristics of the whole material could influence the adsorption process.

Conclusions

Inner and outer portions of SCB have different characteristics. Its composition varies because the presence of lignin, cellulose, and hemicellulose is different, which also makes a difference between its chemical surfaces. There are more base groups than the acidic groups in all cases and, therefore, the surface is negatively charged. The pH_{ZCP} is lower than 7 for all materials, and at the same time lower than the final pH (after the atrazine adsorption). This last helps with the adsorption

of copper ions. The morphology of the external portion is more porous than the internal portion and this last one has layers covering channels, structures such as comb could be observed. The characteristics could be modified due to the treatment conditions. SEM images showed morphologically differences between external and internal SCB. Unusual debris found in the natural SGB suggests that a material pretreatment is necessary before it can be used. Subsequently, SEM images showed that the pretreatment with sodium hydroxide solution is more aggressive for the natural structure than pretreatment with ethanol solution and hot water. The Fourier transformed infrared spectroscopy (FTIR) verified changes in each SCB portion after pretreatments related to functional groups of lignocellulosic materials. Mathematical models established a chemical adsorption of copper onto heterogeneous material, where intra-particle diffusion was the rate limiting step of the process in all but one case, film diffusion was the rate limiting step for IB_{Eth}. Equilibrium times ranging from 8 to 24 h were in accordance to the adsorption rate established by pseudo second order model. The XPS analysis confirms that Cu(II) and Cu(I) are present in EB_{OH} and IB_{Eth}. The XPS results show that the copper in the SCB is in the compounds: Cu_2O, $Cu(OH)_2$ and CuO. There is more presence of Cu_2O in EB_{OH} than in IB_{Eth} related to the structure differences between external and internal SCB and pretreatment influence. In general, external SCB treated with a sodium hydroxide solution and internal SCB treated with ethanol solution are promising adsorbent materials for copper removal because they presented the highest adsorption capacities; treatments are not expensive and SCB is a cheap, available and biodegradable material.

References

1. A. Roy, J. Bhattacharya, *Nanotechnology in Industrial Wastewater Treatment*, 1st edn. (IWA Publishing, London, 2015), pp. 11–13
2. G. Coman, C. Draghici, in *Nanotechnology in Industrial Wastewater Treatment*, ed. by L.I. Simeonov, M.V. Kochubovski, B.G. Simeonova (Springer, Sofía, 2010), p. 51
3. S.E. Jorgensen, B.D. Fath, *Ecotoxicology*, 1st edn. (Elsevier, Amsterdam, 2010), p. 219
4. L. Liang, Y.Y. Zhang, H. Lin, in *Environment, Energy and Applied Technology*, ed. by W.P. Sung, J. Kao (Taylor and Francis Group, Leiden, 2015), pp. 21–24
5. S. Rajeshkumar, X. Li, Toxicol. Rep. **5**, 288 (2018)
6. CONADESUCA, (Gobierno de Mexico, 2017)
7. P.C. Brandão, T.C. Souza, C.A. Ferreira, C.E. Hori, L.L. Romanielo, J. Hazard. Mater. **175**, 1106 (2010)
8. L.R. Martins, J.A. Vieira, O.F. Herrera, T.M. Sacramento, L.V. Alves, L. Frédéric, J. Colloid Interface Sci. **494**, 223 (2017)
9. K. Anoop Krishnan, T.S. Anirudhan, Ind. Eng. Chem. Res. **41**, 5085 (2002)
10. S.A. Saad, K.M. Isa, R. Bahari, Desalination **264**, 123 (2010)
11. O.K. Júnior, L.V. Alves Gurgel, R. Pereira de Freitas, L.F. Gila, Carbohydr. Polym. **77**, 643 (2009)
12. V.G. Dos Santos, J.V. De Souza, C.R. Tarley, J. Caetano, D. Cardoso Dragunski, Water Air Soil Pollut. **216**, 351 (2011)

13. P.C. Siu, L.F. Koong, J. Saleem, J. Barford, G. McKay, Chin. J. Chem. Eng. **24**, 94 (2016)
14. E. Ntagia, P. Rodenas, A. Heijne, C.N. Buisman, T.J. Sleutels, Int. J. Hydrogen Energy **41**, 5758 (2016)
15. L. Ye, L. Chai, Q. Li, X. Yan, Q. Wang, H. Liu, RSC Adv. **6**, 114405 (2016)
16. D.K. Bai, Q.H. Ying, N. Wang, J.H. Lin, J. Chem. **2016**, 1 (2016)
17. E.M. Soliman, S.A. Ahmed, A.A. Fadl, Arab. J Chem. **4**, 63 (2011)
18. S. De, A. Maiti, *Arsenic Removal from Contaminated Groundwater* (The Energy and Resources Institute, New Delhi, 2012), p. 93
19. E.M. Azzam, G. Eshaq, A.M. Rabie, A. Bakr, A.A. Abd-Elaal, A. El Metwally, Int. J. Biol. Macromol. **89**, 507 (2016)
20. H. Beheshti, M. Irani, L. HosseinI, A. Rahimi, M. Aliabadi, Chem. Eng. J. **284**, 557 (2016)
21. T.T. Hong, H. Okabe, Y. Hidaka, K. Hara, Carbohydr. Polym. **157**, 335 (2017)
22. A. Moubarik, N. Grimi, Food Res. Int. **73**, 169 (2015)
23. P.J. Van Soest, J.B. Roberson, B.A. Lewis, J. Dairy Sci. **74**, 3583 (1991)
24. A. Blanco-Flores, A. Colín-Cruz, E. Gutiérrez-Segura, V. Sánchez-Mendieta, D. Solís-Casados, M. Garrudo-Guirado, R. Batista-González, Environ. Technol. **35**, 1508 (2014)
25. C. Wang, H. Ge, Y. Zhao, S. Liu, Y. Zou, W. Zhang, J. Magn. Magn. Mater. **423**, 421 (2017)
26. F. Machado, E.C. Lima, I.M. Jauris, M. Adebayo, in *Carbon Nanomaterials as Adsorbents for Environmental and Biological Applications*, ed. by C. Bergmann, F. Machado (Springer, Cham, 2015), pp. 85–105
27. J.L. Guimarães, E. Frollini, C.G. Da Silva, F. Wypych, K.G. Satyanarayana, Ind. Crop. Prod. **30**, 407 (2009)
28. Z. Zhang, L. Moghaddam, I.M. O'Hara, W.O. Doherty, Chem. Eng. J. **178**, 122 (2011)
29. M.V. Rapp, G.P. Maier, H.A. Dobbs, N.J. Higdon, J.H. Waite, A. Butler, J.N. Israelachvili, J. Am. Chem. Soc. **138**, 9013 (2016)
30. L. Toscano Palomar, A.G. Ayala Bautista, G. Montero Alpirez, L. Cervantes Díaz, R. Torres Ramos, E. Romero Uscanga, M.G. Amado Moreno, Á. García Velázquez, Rev. Ciencia Tecnol. **15**, 113 (2015)
31. E.S. Abdel-Halim, Arab. J. Chem. **7**, 362 (2014)
32. J. Salcedo Mendoza, J. Galán López, L.M. Pardo Flórez, Rev. Colomb. Biotecnol. **14**, 171 (2018)
33. L. Mesa, E. González, E. Ruiz, I. Romero, C. Cara, F. Felissia, E. Castro, Appl. Energy **87**, 109 (2010)
34. Y.R. Loh, D. Sujan, M.E. Rahman, C.A. Das, Resour. Conserv. Recycl. **75**, 14 (2013)
35. P.F. Pereira, H.C. Voorwald, M.C. Da Silva, A.B. Rego, A.A. Ferraria, M.N. De Pinho, Cellulose **21**, 641 (2014)
36. T. Zhong, G.S. Oporto, Y. Peng, X. Xie, D.J. Gardner, Cellulose **22**, 2665 (2015)
37. S. Malamis, E. Katsou, J. Hazard. Mater. **252**, 428 (2013)
38. S.S. Gupta, K.G. Bhattacharyy, Adv. Colloid Interface Sci. **162**, 39 (2011)
39. C. Tejada, A. Herrera, E. Ruiz, Ing. Compet. **18**, 117 (2016)
40. H. Uslu, S. Majumder, J. Chem. Eng. **62**, 1501 (2017)
41. H. Mittal, A. Maity, S.S. Ray, Int. J. Biol. Macromol. **79**, 8 (2015)
42. B. Noroozi, G.A. Sorial, J. Hazard. Mater. **139**, 167 (2007)
43. R.K. Gupta, E. Kennel, K.J. Kim, *Polymer Nanocomposites* (Taylor and Francis, Boca Raton, 2010), p. 48
44. G. Trefalt, S. Behrens, M. Borkovec, Langmuir **32**, 380 (2015)
45. T. Bhagavathi Pushpa, J. Vijayaraghavan, S.J. Sardhar Basha, V. Sekaran, J. Jegan, Ecotoxicol. Environ. Safe. **118**, 177 (2015)
46. Y.A. El-Reash, A.M. Abdelghany, A.A. Elrazak, Int. J. Biol. Macromol. **86**, 789 (2016)
47. J.X. Yu, R.A. Chi, Y.F. Zhang, Z.G. Xu, C.Q. Xiao, J. Guo, Bioresour. Technol. **110**, 160 (2012)
48. M. Iqbal, R.A. Khera, Chem. Int. **1**, 157 (2018)
49. H. Gupta, P.R. Gogate, Ultrason Sonochem. **30**, 113 (2016)
50. S. Ben-Ali, I. Jaouali, S. Souissi-Najar, A. Ouederni, J. Clean. Prod. **142**, 3809 (2016)

Affiliations

Helen P. Toledo-Jaldin[1] · Alien Blanco-Flores[3,4] ·
Gustavo López-Téllez[2] · Alfredo R. Vilchis-Nestor[2] ·
Víctor Sánchez-Mendieta[2] · Ernesto Morales-Almaraz[5] ·
Luis Alberto Mejía-Uribe[5]

[1] Posgrado en Ciencia de Materiales, Facultad de Química, Universidad Autónoma del Estado de México Paseo Colón y Tollocan, C.P. 50110 Toluca, Mexico State, Mexico

[2] Centro Conjunto de Investigación en Química Sustentable UAEM-UNAM, (CCIQS), Carretera Toluca-Atlacomulco Km 14.5, Unidad El Rosedal, C.P. 50200 Toluca, Mexico State, Mexico

[3] División de Ingeniería Mecánica, Tecnológico de estudios superiores de Tianguistenco, Carretera Tenango-La Marqueza, Km 22, Santiago Tilapa, C.P. 52650 Santiago Tianguistenco, Mexico

[4] Instituto de Metalurgia, Universidad Autónoma de San Luis Potosí, Av. Sierra Leona 550, Lomas 2da Sección, C.P. 78210 San Luis Potosí, Mexico

[5] Departamento de Nutrición Animal, Facultad de Medicina Veterinaria y Zootecnia, Universidad Autónoma del Estado de México, El Cerrillo Piedras Blancas, C.P. 50090 Toluca, Mexico State, Mexico